



1 **Topographic modulation on the layered circulation in South China Sea**

2

3

4

Qibang Tang^{1,2}, Zhongya Cai^{1,2}, Zhiqiang Liu³

5 1 State Key Laboratory of Internet of Things for Smart City, Department of Ocean Science and
6 Technology, University of Macau, China

7 2 Centre of Ocean Research in Hong Kong and Macau (CORE), Hong Kong, China

8 3. Department of Ocean Science and Engineering and Center for Complex Flows and Soft
9 Matter Research, Southern University of Science and Technology, Shenzhen, China

10

11 *Correspondence to:* Zhongya Cai (zyc@um.edu.mo)

12

13

14

15



16

17 **Abstract:** The South China Sea (SCS) is the largest semi-enclosed marginal sea in western
18 Pacific. It exhibits a unique vertically rotating cyclonic, anticyclonic, and cyclonic circulation
19 in its upper, middle, and deep layers. Over slope topography, these layered currents interact and
20 significantly shape the structure and intensity of the basin circulation. In this study, we employ
21 process-oriented numerical simulations to investigate how upper-layer processes, characterized
22 by greater magnitude and variability, influence the layered circulation over the irregular
23 topographic slope. The simulations reveal that stronger upper intrusion from open ocean
24 directly enhances upper layer circulation, which subsequently strengthens the middle and the
25 deep slope currents. Vorticity dynamics illustrate that changes in the middle and deep slope
26 current are largely related to the vertical stretching (ζ_{DIV}) induced by bottom geostrophic
27 cross-isobath transport (CGT_b). As the upper-layer cyclonic slope current intensifies, it
28 modulates the bottom pressure distribution, resulting in stronger negative ζ_{DIV} predominantly
29 over the northwestern slope to intensify the middle anticyclone slope current. Similarly, for the
30 deep cyclonic slope current, the CGT_b maintains downward cascading in the northern part and
31 upwelling over the southern slope. Over the southern slope, the strengthening of the positive
32 CGT_b is induced by the increment of the advection of relative vorticity and planetary vorticity
33 in water column, in which the middle layer provides approximately 40% of the total
34 strengthening trend, but the upper layer has a minimal impact. Conversely, on the northern
35 slope, the strengthening of the negative CGT_b is primarily influenced by the upper layer.

36

37 **Keywords:** Circulation dynamics; Layered circulation; Process-oriented simulation;
38 Topographic modulation; Vertical coupling

39



40 **1. Introduction**

41

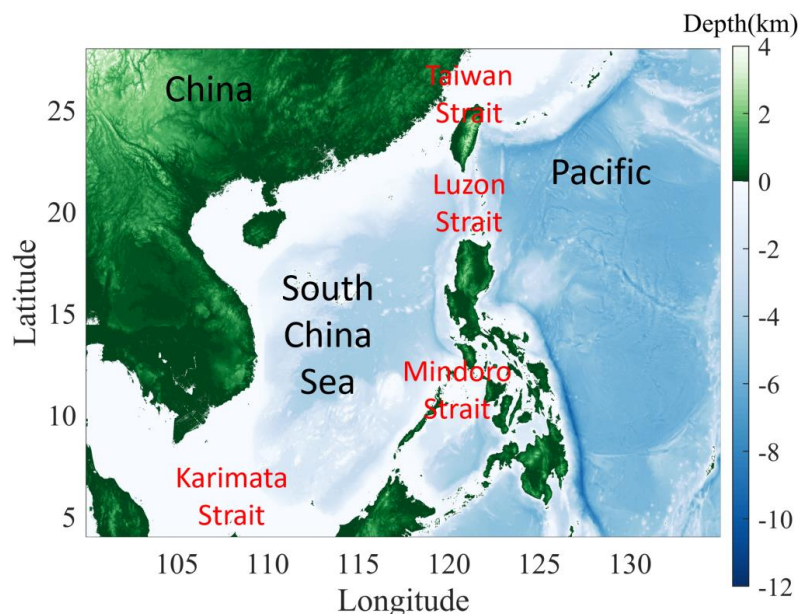
42 Marginal seas circulation plays crucial role in the mass transport and regional climate
43 dynamics, with circulation patterns being strongly influenced by their unique topographic
44 features (Milot 1999, Omstedt, Elken et al. 2004, Oey, Ezer et al. 2005, Gan, Li et al. 2006,
45 Johns and Sofianos 2012). This topographic regulation results in intricate layered slope currents
46 that flow in different directions at various depths (Yuan 2002, Wang, Xie et al. 2011, Lan, Zhang
47 et al. 2013, Gan, Kung et al. 2022). These layered currents interact over slope topography,
48 significantly shaping the structure and intensity of the overall circulation (Gan, Liu et al. 2016,
49 Quan and Xue 2018). For instance, in the Gulf of Mexico, loop current eddies influence not
50 just the upper-layer circulation but also the deep flow, illustrating the importance of vertical
51 coupling in transferring energy and variability to deeper currents (Tenreiro, Candela et al. 2018).
52 Understanding these dynamics helps elucidate the behavior of marginal sea's circulation (Liang,
53 Spall et al. 2017, Zhu and Liang 2020, Olvera-Prado, Moreles et al. 2023).

54 The South China Sea (SCS) is the largest semi-enclosed marginal sea located in the
55 tropical region. It exhibits a unique mean cyclonic, anticyclonic, and cyclonic (CAC)
56 circulation in its upper, middle, and deep layers (Wang, Xie et al. 2011, Shu, Xue et al. 2014,
57 Lan, Wang et al. 2015, Gan, Liu et al. 2016, Zhu, Sun et al. 2017). The strong upper layer
58 circulation is driven by the Asia monsoon and Kuroshio intrusion from Luzon Strait (LS), while
59 the middle and deep circulations are maintained by the outflux and deep intrusion through LS,
60 respectively. Over the slope topography, the CAC circulation affects each other through the
61 vertical coupling among them (Shu, Wang et al. 2018). For example, the study of Quan and
62 Xue (2018) demonstrated that perturbations in the upper layer can transit through the water
63 column and affect deeper circulation by altering layer thickness. This coupling is particularly
64 evident over the strong boundary current that in the northern basin and along the western
65 boundary. Numerical experiments by Wang et al. (2018) suggest that, although the basin-scale
66 circulation is primarily driven by the LS overflow, upwelling patterns are essential in shaping
67 the detailed structure of the deep-water circulation. Similar processes have been observed in
68 other marginal seas as well (e.g., Testor et al., 2018; Wang et al., 2024; Xu et al., 2009; Olvera-
69 Prado, Moreles et al. 2023).

70 Despite advances in understanding the major features of mean layered circulation, the
71 response of this circulation to changes in external forcings—particularly the strong upper ocean
72 processes—and the specific mechanisms involved remain poorly understood. A comprehensive
73 understanding of how topographically modulated vertical coupling over basin slopes influences
74 the structure and intensity of mean circulation is crucial for exploring the long-term evolution
75 of marginal sea circulation. For instance, Kuroshio intrusion has been observed to weaken with



76 decadal variations, while upper ocean currents have shown acceleration in response to a
77 warming climate (Peng et al., 2022; Chen et al., 2019; Nan et al., 2013). How the layered
78 circulation in marginal seas responds to these changes remains unclear. This study employs
79 process-oriented simulations to elucidate how upper-layer processes, which exhibit greater
80 intensity and variability, influence layered circulation over the meandering bottom slope in the
81 SCS. The paper is organized as follows: Section 2 explains the configuration of the simulation.
82 Section 3 offers the response of layered slope current intensity to the changes of the upper
83 circulation. Section 4 explores the underlying physical mechanisms. Finally, Section 5 provides
84 a summary of our findings.



85
86 **Figure 1.** Location and bathymetry (km) of the South China Sea, showing Luzon Strait, Taiwan
87 Strait, Mindoro Strait, and Karimata Strait.

88 89 90 **2. Methodology**

91 Based on the Regional Ocean Modeling System (ROMS) (Shchepetkin & McWilliams,
92 2005), we performed a three-dimensional process-oriented simulation in this study (Cai et al.,
93 2023). The model setup included a circular basin on the west representing the SCS and a
94 rectangular basin on the east representing the Western Pacific Ocean, connected by a narrow
95 strait (representing the Luzon Strait, LS) with a depth of 2500 m. The slope in the SCS increases
96 from 400 to 4000 m and the central basin has the depth of 4000 m.

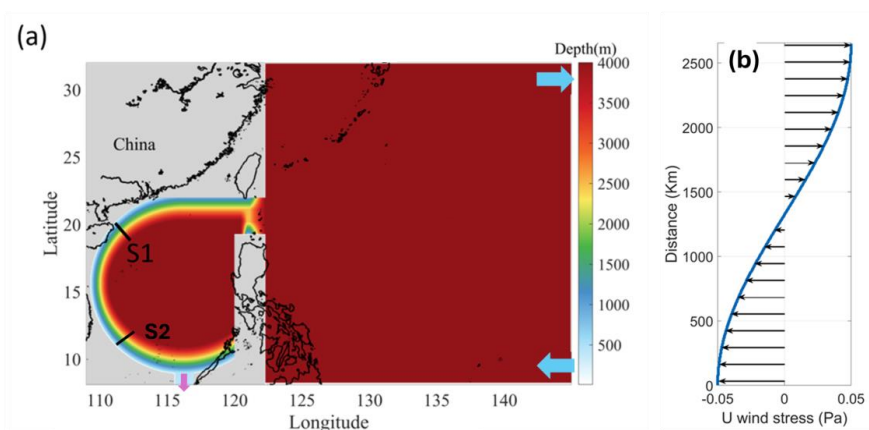
97 The model employed a uniform horizontal grid with a 5 km resolution, and the vertical



98 structure utilized stretched, terrain-following coordinates with 30 layers (Song and Haidvogel
99 1994) were adopted with 30 layers. In the upper layer, the influx/outflux was defined at the
100 southeastern (25 Sv) and northeastern (20 Sv) boundaries of the open ocean, and the SCS had
101 an opening to the south to allow for outflux (Figure 2a), consequently, the intrusion from open
102 ocean into SCS will be generated. The model incorporated variable mixing coefficients (K_v) to
103 simulate differences in exchange currents between the SCS and the Western Pacific Ocean,
104 particularly in the middle and deep parts of the LS (Tian, Yang et al. 2009, Yang, Zhao et al.
105 2016). In the SCS and the western half of the LS, K_v values were set as $5 \cdot 10^{-4} m^2 s^{-1}$ between
106 500 and 1,500 m, $2 \cdot 10^{-3} m^2 s^{-1}$ below 1,500 m, and $5 \cdot 10^{-3} m^2 s^{-1}$ in the layer 500 m from the
107 bottom. In the upper 500 m of SCS and LS, and throughout the entire water column of the open
108 ocean, a background K_v of $2 \cdot 10^{-5} m^2 s^{-1}$ was applied. A zonal wind stress with meridional
109 variations was applied over the open ocean, while the atmospheric buoyancy flux over the SCS
110 was simplified by setting it to zero.

111 The model was initialized with horizontally uniform temperature and salinity profiles
112 derived from the mean data of the World Ocean Atlas, averaged over the region west of the LS.
113 The simulation ran for 25 years, and the analysis was conducted on the results from the final 5
114 years.

115



116

117

118 Figure 2. (a) The topography and geometry used in the idealized process-oriented simulation.
119 The black lines show the realistic surrounding coastline. S1 and S2 are two vertical sections for
120 showing slope current. (b) Distribution of the wind stress.

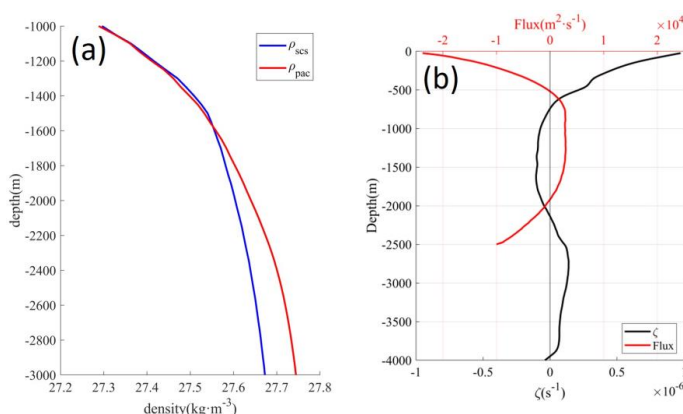
121

122 3. Results

123 In the LS, the influx occurs in the upper and deep layers, while the outflux occurs in the
124 middle layer between them (Figure 3b). The upper intrusion is intrinsically linked to the western



125 boundary current in the open ocean, i.e. Kuroshio Current, while the exchange currents in the
 126 middle and bottom layers are primarily related to the density differences between the South
 127 China Sea (SCS) and the Pacific (Zhu et al., 2017, 2019; Cai, Chen et al. 2023; Zhou et al.,
 128 2023). Under the density difference, the westward pressure gradient was formed that drives the
 129 deep intrusion from the open ocean towards the SCS (Wang, Xie et al. 2011). Associated with
 130 the stimulated layered exchanging current, the horizontally averaged vorticity features with the
 131 positive-negative-positive values in the respective depth of the basin, which represent the
 132 cyclonic, anticyclonic and cyclonic slope current (Figure 3b).



133

134 Figure 3. (a) Vertical profile of domain averaged density ρ (kg·m⁻³) in SCS and Pacific between
 135 1000m to 3000m. (b) Black line shows the vertical profile of the SCS basin-averaged vorticity
 136 (s⁻¹) and the red line shows the flux through LS (m²·s⁻¹). The positive/negative vorticity
 137 represents the cyclonic/anticyclonic circulation, and the positive/negative value flux represents
 138 the outflux/influx through LS.

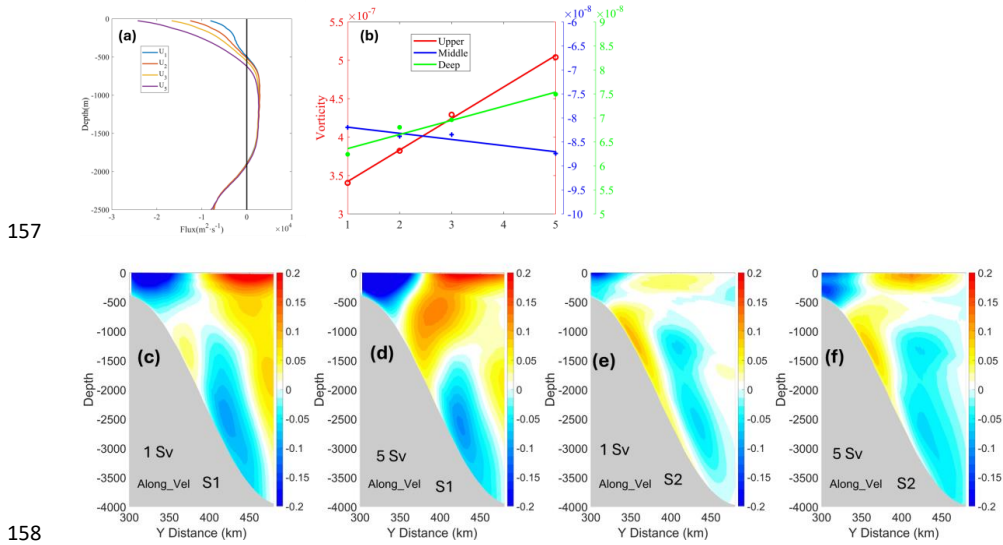
139

140

141 To investigate how the changes in upper layer current modulates the layered circulation,
 142 additional numerical experiments were conducted by adjusting the northeastern outflux to 22Sv,
 143 23Sv and 24Sv, thus the upper LS intrusion was adjusted to 3Sv (Case_U3), 2Sv (Case_U2)
 144 and 1Sv (Case_U1). In these scenarios, the middle and deep exchanging currents, which were
 145 primarily sustained by the contrasting densities between the SCS and the open ocean, remained
 146 relatively unchanged (Figure 4a). Inside the basin, the enhancement of the upper layer inflow
 147 directly intensified the upper layer cyclonic circulation (Figure 4 c-f). And subsequently
 148 strengthened the middle anticyclonic slope current, particularly in the northwestern part of the
 149 basin (transect S1, Figure 4c, d). Additionally, although not directly connected to the upper
 150 layer, the deep cyclonic slope current also exhibited increased strength (Figure 4c-f). Using the
 151 domain-averaged vorticity as an indicator, it was observed that the intensification of the upper
 152 layer circulation resulted in a 10% increase in the intensity of the middle anticyclonic



153 circulation and a 27% increase in the deep cyclonic circulation (Figure 4b). Given that only the
 154 upper layer circulation is directly amplified by the upper intrusion, the remote influence from
 155 upper layer processes over the basin slope significantly impacts the intensity of the layered
 156 circulation, which was explored below.



160 **Figure 4.** (a) Vertical profile flux across the LS under varying upper layer influx. (b) Changes
 161 in the basin-averaged vorticity between 0-500 m (Upper), 1000-2000 m (Middle) and 3000-
 162 4000 m (Deep) with different upper influx. (c-f) The along-slope current ($m \cdot s^{-1}$) over the
 163 section S1 and S1 in Standard case (upper intrusion is 5 Sv) and Case_U1 (upper LS intrusion is
 164 1Sv), respectively. The locations of the two transects are shown in Figure 1a. The transect
 165 locations are indicated in Figure 1a. Positive values represent anticyclonic flow, while negative
 166 values indicate cyclonic flow.

167

168

169 4. Discussion

170

171 To understand how the upper layer processes modulate the layered current over the slope,
 172 we first investigated the layered-integrated vorticity budget for each layer (Gan, Liu et al. 2016,
 173 Cai, Chen et al. 2023):

$$\begin{aligned}
 & \overbrace{\int_A [\nabla \times \int_{layer} (PGF) dz] dA}^{\zeta_{PGF}} + \overbrace{\int_A [\nabla \times \int_{layer} (ADV) dz] dA}^{\zeta_{ADV}} + \overbrace{\int_A [-f \nabla \cdot \int_{layer} (\vec{V}_h) dz] dA}^{\zeta_{COR}} + \overbrace{\int_A [-\beta \cdot \int_{layer} (v) dz] dA}^{\zeta_{BETA}} + \\
 & \overbrace{\int_A [\nabla \times \int_{layer} (VIS) dz] dA}^{\zeta_{VIS}} = 0 \quad (1)
 \end{aligned}$$

174
175

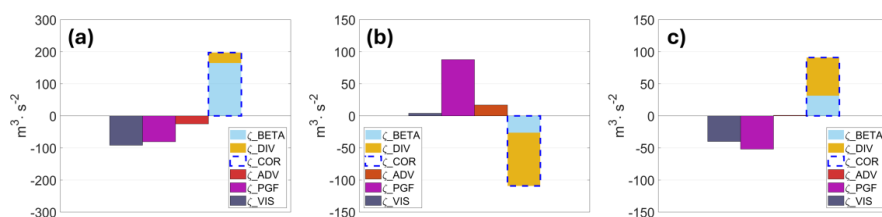
176 where PGF is pressure gradient force, ADV is nonlinear advection, VIS is the turbulent
 177 viscosity. COR is the Coriolis force and the domain-integrated ζ_{COR} represents the lateral



178 planetary vorticity flux. Inside the basin, the ζ_{COR} can be further decomposed into the
 179 vertical stretching induced by the divergence of the horizontal flow (ζ_{DIV}) and β effect of the
 180 meridional current (ζ_{BETA}).

181 The circulation in SCS is primarily governed by geostrophic balance, manifested as
 182 ζ_{COR} balanced by the ζ_{PGF} in both layers. It suggests that the mean cyclonic/anticyclonic
 183 circulation is related to the lateral planetary vorticity influx/outflux (Figure 5) (Cai and Gan
 184 2019, Cai, Chen et al. 2023; Zhu et al., 2017, 2019). Consequently, the strengthening of the
 185 upper LS intrusion directly intensifies the upper layer cyclonic slope current by providing more
 186 positive planetary vorticity flux. In the semi-enclosed middle and deep layers, the vorticity
 187 input is mainly provided by the ζ_{DIV} , as also highlighted in the previous studies (Zhu, Sun et
 188 al. 2017, Wang, Du et al. 2018, Cai, Chen et al. 2023). The positive ζ_{DIV} in the upper and
 189 deep layers reflects the downward and upward flux, which squeeze the middle layer and provide
 190 the negative vertical flux (negative ζ_{DIV}) for the anticyclonic circulation. Therefore, the
 191 intensification of the middle and deep slope currents is largely attributed to vertical stretching
 192 over the basin slope.

193



194

195

196 **Figure 5.** The layered-integrated vorticity budget (Equation 1) for the standard case in the layers of (a)
 197 0–500, (b) 1,000–2,000, and (c) 2,500–4,000 m.

198

199

200 **a. Intensification of middle anticyclonic slope current**

201

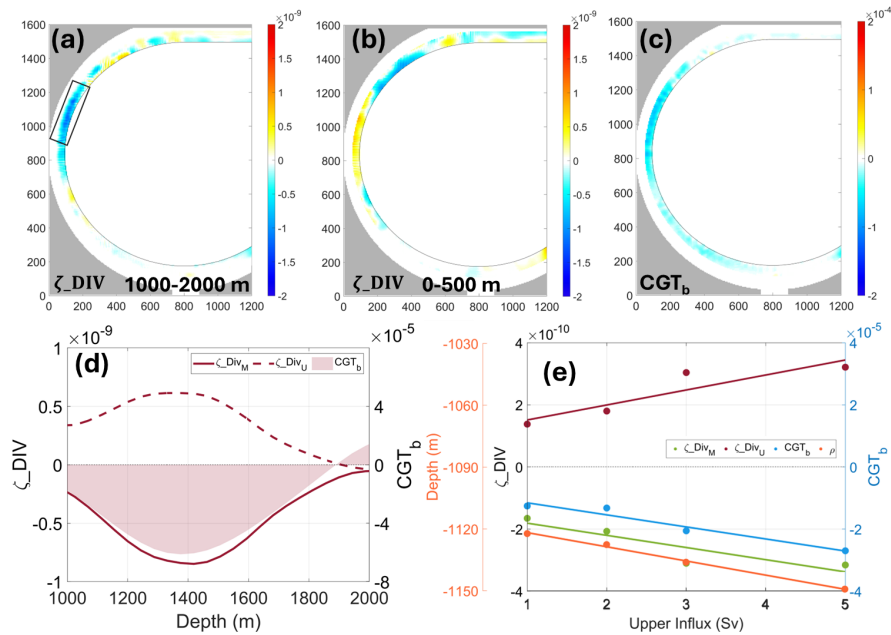
202 For the middle anticyclonic slope current, the negative middle-layered ζ_{DIV} (ζ_{DIV_M})
 203 mainly occurs over the northwestern slope (Figure 6a), where a relatively strong anticyclonic
 204 slope current is observed. In this area, the upper layer generally exhibits positive ζ_{DIV}
 205 (ζ_{DIV_U}), indicating downward squeezing from the upper layer that helps maintain the middle
 206 anticyclonic slope current (Figure 6 b). The increased squeezing from the upper slope current
 207 is expected to intensify the middle anticyclonic slope current (Figure 4 c, d). Since the
 208 stretching/squeezing imposed on the slope current is closely related to the vertical motion
 209 (Liang, Spall et al. 2017), the mean vertical motions over the slope can be understood as follows:



$$\bar{w} = -\nabla_h \cdot \int_{-H}^z \bar{\vec{V}}_h dz \approx -\nabla_h \cdot \int_{-H}^z \bar{\vec{V}}_{h_geo} dz = -\overbrace{(\bar{v}_{b_geo} H_y + \bar{u}_{b_geo} H_x)}^{CGT_b} + \underbrace{\frac{\beta}{f} \int_{-H}^z \bar{v}_{geo} dz}_{\beta \text{ effect}} \quad (2)$$

211 where H is the topography, $_geo$ represents the geostrophic component of the horizontal
 212 current, which is maintained by the distribution of bottom pressure. H_x and H_y are the
 213 horizontal gradients of the bottom slope, \bar{u}_{b_geo} and \bar{v}_{b_geo} are the bottom geostrophic currents.
 214 When the current flows over the slope, the bottom pressure distribution interacts with the
 215 meandering topography and the resulting geostrophic cross-isobath transport (CGT_b) to
 216 influence the vertical motions over the slope. Generally, the CGT_b largely governs the mean
 217 vertical motion over northwestern slope, which in turn squeezes and stretches the middle and
 218 upper slope currents. This process is crucial in maintaining the vorticity input through ζ_DIV
 219 (Figure 6 d), thereby sustaining the dynamics of the slope currents.

220 Associated with the intensification of the upper layer cyclonic slope current, the stronger
 221 slope current modulates the bottom pressure distribution over the slope, leading to stronger
 222 vertical squeezing (ζ_DIV) within the water column. The increase in squeezing gradually
 223 deepens the isopycnal surface and strengthens the middle anticyclonic slope current (Figure 6e).
 224



225

226 **Figure 6.** (a-c) ζ_DIV integrated between 1000-2000 m (ζ_DIV_M), 0-500 m (ζ_DIV_U), and
 227 CGT_b over the region of middle anticyclonic slope current between 1000-2000 m. The black
 228 line indicates the 2000 m isobath line. (d) Change of the ζ_DIV integrated between 100-2000 m
 229 (ζ_DIV_M), between 0-500 m (ζ_DIV_U) with the depth over the northwestern slope. (e) Changes
 230 of the ζ_DIV_M , ζ_DIV_U , CGT_b and the depth of isopycnal surface of 1027.4 kg/m³ with different



231 upper LS influx. (d) and (e) was plotted using the data averaged over the region of black box
232 in (a)

233

234

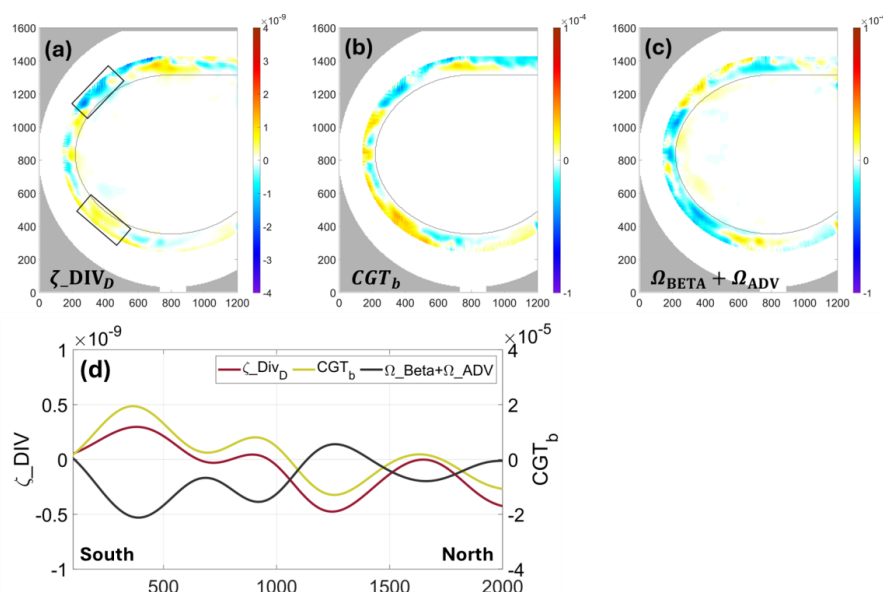
235 **b. Intensification of the deep cyclonic slope current**

236 For the deep cyclonic slope current, the deep ζ_{DIV} (ζ_{DIV_D}) features a downward flux
237 (negative value) over the northern slope and upward flux (positive value) over the southern part
238 (Figure 7a, d). This pattern aligns with the classical source-sink driven theory (Stommel and
239 Arons 1959; Yuan et al., 1997), which suggests the sinking from the northern basin and
240 upwelling from the southern basin would sustain the abyssal cyclonic circulation. Same as the
241 middle anticyclonic slope current, the ζ_{DIV_D} is largely controlled by the CGT_b that the
242 pressure distribution maintained the mean cascading in the northern side and the upwelling over
243 the southern slope (Figure 7b, d). To explain the maintenance of the bottom pressure
244 distribution, the vertical integrated vorticity dynamic was employed (Gan, Liang et al. 2013,
245 Cai and Gan 2021):

$$246 \quad \overbrace{\nabla \times \int_{-H}^0 (\overrightarrow{PGF}) dz}^{\Omega_{PGF}} + \overbrace{\nabla \times \int_{-H}^0 (\overrightarrow{ADV}) dz}^{\Omega_{ADV}} + \underbrace{\beta \int_{-H}^0 v dz}_{\Omega_{BETA}} - \overbrace{\nabla \times \int_{-H}^0 (\overrightarrow{VIS}) dz}^{\Omega_{VIS}} = 0 \quad (3)$$

247 Where $\Omega_{PGF} = \nabla \times \int_{-H}^0 (\overrightarrow{PGF}) dz = -(\bar{v}_{b_geo} H_y + \bar{u}_{b_geo} H_x)$, thus represents the effect of CGT_b .
248 It illustrates that the bottom pressure distribution is maintained by the nonlinear advection of
249 relative vorticity (Ω_{ADV}), advection of planetary vorticity (Ω_{BETA}), and net viscosity of the
250 current flowing over the slope topography. Among them, the Ω_{BETA} and Ω_{ADV} play the
251 major role in sustaining the bottom pressure distribution of the deep cyclonic slope current
252 (Figure 8 c, d).

253

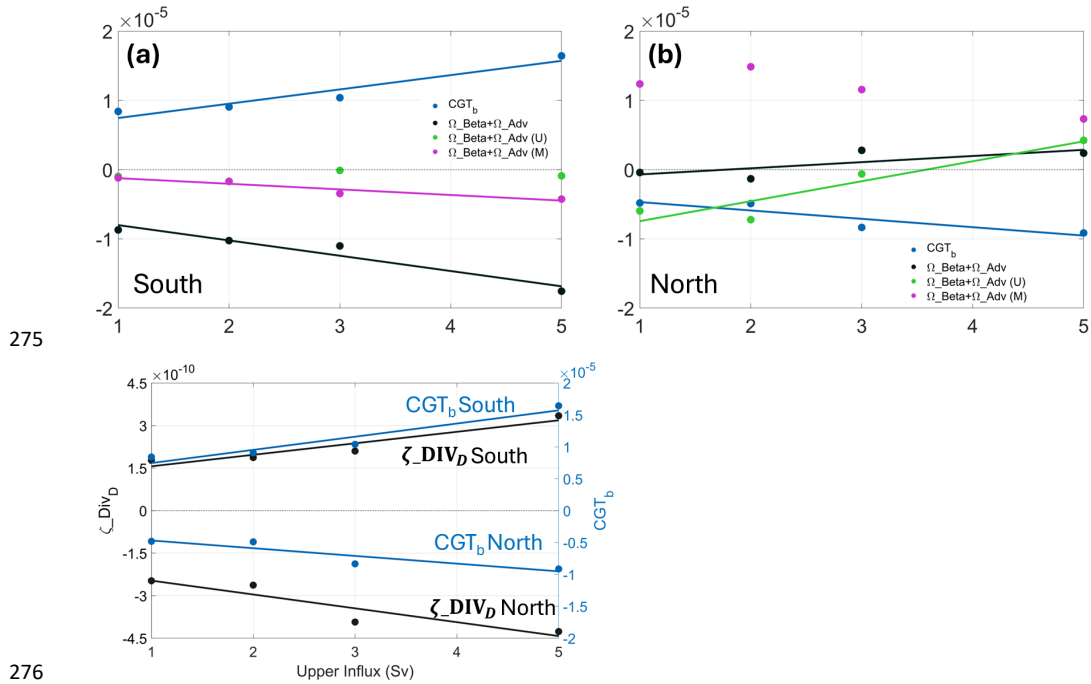


254

255

256 Figure 7 (a-c) ζ_{DIV} integrated below 3000 m of the deep cyclonic slope current (ζ_{DIV_D}),
 257 CGT_b and $\Omega_{BETA} + \Omega_{ADV}$ over the region of middle anticyclonic slope current below 3000
 258 m. The black line indicates the 4000 m isobath line. (d) Meridional changes of the ζ_{DIV_D} ,
 259 CGT_b and $\Omega_{BETA} + \Omega_{ADV}$ over the slope.
 260

261 As the upper intrusion intensifies, the bottom pressure distribution adjusts in response to
 262 changes in the layered circulation, resulting in a gradual strengthening of the negative
 263 CGT_b over the northern slope and positive CGT_b over the southern part (Figure 8 a-b). Over the
 264 southern slope (Figure 8a), the strengthening of the positive CGT_b is induced by the increase of
 265 the $\Omega_{BETA} + \Omega_{ADV}$ in the water column, in which the middle layer [$\Omega_{BETA} + \Omega_{ADV}$ (M)]
 266 provides approximately 40% of the total strengthening trend, while the upper layer [Ω_{BETA}
 267 $+ \Omega_{ADV}$ (U)] has a negligible impact. Conversely, over the northern slope, the strengthening
 268 of the $\Omega_{BETA} + \Omega_{ADV}$ is primarily influenced by the upper layer, with the middle layer has
 269 the negative effect (Figure 8b). Thus, the intensification of downward CGT_b over the northern
 270 slope is directly modulated by the strengthening of the upper cyclonic slope current, while the
 271 intensification of upward CGT_b over the southern slope is mainly driven by the strengthening
 272 of the middle anticyclonic slope current. These changes in CGT_b enhance deep stretching,
 273 thereby strengthening the deep cyclonic slope current accordingly (Figure 8c).
 274



275

276

277

278 **Figure 8.** (a) Changes of the CGT_b , $\Omega_{Beta} + \Omega_{Adv}$ in the total water column, $\Omega_{Beta} + \Omega_{Adv}$ in the
 279 layer between 0-500 m ($\Omega_{Beta,U} + \Omega_{Adv,U}$), $\Omega_{Beta} + \Omega_{Adv}$ in the between 1000-2000 m
 280 ($\Omega_{Beta,M} + \Omega_{Adv,M}$) over the southern slope (black box in Figure 8a). (b) same as (a) but over
 281 the northern slope (black box in Figure 8a). (c) Change of the CGT_b and ζ_{DIV_D} over the
 282 northern and southern slope.
 283

283

284

285 5. Summary

286 Marginal sea circulation plays a crucial role in mass transport and regional climate
 287 dynamics. Through process-oriented numerical simulations, we examined how upper-layer
 288 processes, which are characterized by greater intensity and variability, impact the layered
 289 circulation over the meandering bottom slope in SCS. The results underscore the intricate
 290 balance between topographical features and oceanic circulation, offering valuable insights for
 291 predicting the behavior of marginal sea circulation under varying forcings conditions

292 The numerical experiments show that the stimulated layered exchange currents through
 293 the LS introduce lateral planetary vorticity flux and facilitate the development of a layered basin
 294 circulation within the SCS. Inside the basin, the intensification of upper-layer inflow directly
 295 enhances the upper-layer cyclonic circulation, which in turn strengthens the middle anticyclonic
 296 slope current, particularly in the northwestern part of the basin. Furthermore, even though the
 297 deep cyclonic slope current is not directly connected to the upper layer, it also exhibits increased



298 strength. Using domain-averaged vorticity as an indicator, it was found that the intensification
299 of the upper-layer circulation resulted in a 10% increase in the intensity of the middle
300 anticyclonic circulation and a 27% increase in the deep cyclonic circulation.

301 The vorticity dynamics illustrate that the changes in the middle and deep slope current is
302 largely related to the vertical stretching over the slope (ζ_{DIV}). When the current flows over
303 the slope, the bottom pressure distribution interacts with the meandering topography and the
304 resulting geostrophic cross-isobath transport (CGT_b) influences the vertical motions. For the
305 middle anticyclonic slope current, the negative middle ζ_{DIV} predominantly occurs over the
306 northwestern slope, where a relatively strong anticyclonic slope current is present. As the upper-
307 layer cyclonic slope current intensifies, it modulates the bottom pressure distribution over the
308 slope, providing stronger vertical squeezing ζ_{DIV} within the water column, which gradually
309 strengthens the middle anticyclonic slope current. For the deep cyclonic slope current, the deep
310 ζ_{DIV} is also largely controlled by the CGT_b over the slope, with the pressure distribution
311 maintaining cascading flows in the northern part and upwelling over the southern slope. Over
312 the southern slope, the strengthening of the positive CGT_b is induced by the increase of the
313 nonlinear advection of relative vorticity and planetary vorticity in the entire water column, in
314 which the middle layer provides approximately 40% of the total strengthening trend, while the
315 upper layer has a negligible impact. Conversely, on the northern slope, the strengthening of the
316 negative CGT_b is primarily influenced by the upper layer, with the middle layer has the negative
317 effect. The results deepen understanding of the intricate balance between topographical features
318 and layered circulation, which help to improve the predictions of the long-term behavior of
319 marginal sea circulation under varying climatic conditions.

320

321

322 Data availability. All data used in this paper are available at
323 <https://doi.org/10.5281/zenodo.13835538>.

324

325 Author contributions. QT conducted the investigation, developed the methodology, and carried
326 out the writing (original draft preparation). ZC was responsible for the conceptualization,
327 supervision, and writing (review and editing). ZL was responsible for the conceptualization and
328 writing (review and editing).

329

330 Competing interests. The contact author has declared that none of the authors has any
331 competing interests.

332

333



334 *Acknowledgement*

335 This work was supported by National Natural Science Foundation of China
336 (42376024, 42276004), the Science and Technology Development Fund, Macau SAR
337 (File/Project no. 001/2024/SKL), and The Center for Ocean Research in Hong Kong
338 and Macau (CORE, EF014/FST-CZY/2023/HKUST). The work described in this paper
339 was substantially supported by a grant from the Research Grants Council of the Hong
340 Kong Special Administrative Region, China (AoE/P-601/23-N). CORE is a joint
341 research centre for ocean research between Laoshan Laboratory and HKUST. This
342 work was performed in part at the SICCC, which is supported by the SKL-IOTSC,
343 University of Macau.

344

345

346



347 **Reference**

- 348 Cai, Z., D. Chen and J. Gan (2023). "Formation of the layered circulation in South China Sea with the mixing
349 stimulated exchanging current through Luzon Strait." Journal of Geophysical Research: Oceans
350 Cai, Z., D. Chen and J. Gan (2023). "Formation of the Layered Circulation in South China Sea With the Mixing
351 Stimulated Exchanging Current Through Luzon Strait." Journal of Geophysical Research: Oceans **128**(3).
352 Cai, Z. and J. Gan (2019). "Coupled External-Internal Dynamics of Layered Circulation in the South China Sea: A
353 Modeling Study." Journal of Geophysical Research: Oceans **124**(7): 5039-5053.
354 Cai, Z. and J. Gan (2021). "Dynamics of the Layered Circulation Inferred from Kinetic Energy Pathway in the South
355 China Sea." Journal of Physical Oceanography **51**(5): 1671-1685.
356 Gan, J., H. Kung, Z. Cai, Z. Liu, C. Hui and J. Li (2022). "Hotspots of the stokes rotating circulation in a large
357 marginal sea." Nat Commun **13**(1): 2223.
358 Gan, J., H. Li, E. N. Curchitser and D. B. Haidvogel (2006). "Modeling South China Sea circulation: Response to
359 seasonal forcing regimes." Journal of Geophysical Research **111**(C6).
360 Gan, J., L. Liang and H. San Ho (2013). "Dynamics of Intensified Downwelling Circulation over a Widened Shelf
361 in the Northeastern South China Sea." Journal of Physical Oceanography **43**(1): 80-94.
362 Gan, J., Z. Liu and C. R. Hui (2016a). "A Three-Layer Alternating Spinning Circulation in the South China Sea."
363 Journal of Physical Oceanography **46**(8): 2309-2315.
364 Gan, J., Z. Liu, and L. Liang, Numerical modeling of intrinsically and extrinsically forced seasonal circulation in the
365 China Seas: A kinematic study. Journal of Geophysical Research: Oceans, 2016b. 121(7): p. 4697-4715.
366 Johns, W. E. and S. S. Sofianos (2012). "Atmospherically Forced Exchange through the Bab el Mandeb Strait."
367 Journal of Physical Oceanography **42**(7): 1143-1157.
368 Lan, J., Y. Wang, F. Cui and N. Zhang (2015). "Seasonal variation in the South China Sea deep circulation." Journal
369 of Geophysical Research: Oceans **120**(3): 1682-1690.
370 Lan, J., N. Zhang and Y. Wang (2013). "On the dynamics of the South China Sea deep circulation." Journal of
371 Geophysical Research: Oceans **118**(3): 1206-1210.
372 Liang, X., M. Spall and C. Wunsch (2017). "Global Ocean Vertical Velocity From a Dynamically Consistent Ocean
373 State Estimate." Journal of Geophysical Research: Oceans **122**(10): 8208-8224.
374 Millot, C. (1999). "Circulation in the western Mediterranean Sea." Journal of Marine Systems **20**(1-4): 423-442.
375 Oey, L., T. Ezer and H. Lee (2005). "Loop Current, rings and related circulation in the Gulf of Mexico: A review of
376 numerical models and future challenges." Geophysical Monograph-American Geophysical Union **161**: 31.



- 377 Olvera-Prado, E. R., E. Moreles, J. Zavala-Hidalgo and R. Romero-Centeno (2023). "Upper–Lower Layer Coupling
378 of Recurrent Circulation Patterns in the Gulf of Mexico." Journal of Physical Oceanography **53**(2): 533-550.
- 379 Omstedt, A., J. Elken, A. Lehmann and J. Piechura (2004). "Knowledge of the Baltic Sea physics gained during the
380 BALTEX and related programmes." Progress in Oceanography **63**(1-2): 1-28.
- 381 Quan, Q. and H. Xue (2018). "Layered model and insights into the vertical coupling of the South China Sea
382 circulation in the upper and middle layers." Ocean Modelling **129**: 75-92.
- 383 Shchepetkin, A. F. and J. C. McWilliams (2005). "The regional oceanic modeling system (ROMS): a split-explicit,
384 free-surface, topography-following-coordinate oceanic model." Ocean Modelling **9**(4): 347-404.
- 385 Shu, Y., Q. Wang and T. Zu (2018). "Progress on shelf and slope circulation in the northern South China Sea."
386 Science China Earth Sciences **61**(5): 560-571.
- 387 Shu, Y., H. Xue, D. Wang, F. Chai, Q. Xie, J. Yao and J. Xiao (2014). "Meridional overturning circulation in the
388 South China Sea envisioned from the high-resolution global reanalysis data GLBa0.08." Journal of Geophysical
389 Research: Oceans **119**(5): 3012-3028.
- 390 Song, Y. and D. Haidvogel (1994). "A semi-implicit ocean circulation model using a generalized topography-
391 following coordinate system." Journal of Computational Physics **115**(1): 228-244.
- 392 Stommel, H. and A. Arons (1959). "On the abyssal circulation of the world ocean—I. Stationary planetary flow
393 patterns on a sphere." Deep Sea Research (1953) **6**: 140-154.
- 394 Tenreiro, M., J. Candela, E. P. Sanz, J. Sheinbaum and J. Ochoa (2018). "Near-Surface and Deep Circulation
395 Coupling in the Western Gulf of Mexico." Journal of Physical Oceanography **48**(1): 145-161.
- 396 Tian, J., Q. Yang and W. Zhao (2009). "Enhanced diapycnal mixing in the South China Sea." Journal of Physical
397 Oceanography **39**(12): 3191-3203.
- 398 Wang, A., Y. Du, S. Peng, K. Liu and R. X. Huang (2018). "Deep water characteristics and circulation in the South
399 China Sea." Deep Sea Research Part I: Oceanographic Research Papers **134**: 55-63.
- 400 Wang, G., S.-P. Xie, T. Qu and R. X. Huang (2011). "Deep South China Sea circulation." Geophysical Research
401 Letters **38**(5): n/a-n/a.
- 402 Yabal, H. (1983). Continental margin geology. Petroleum Industry Press.
- 403 Yang, Q., W. Zhao, X. Liang and J. Tian (2016). "Three-Dimensional Distribution of Turbulent Mixing in the South
404 China Sea." Journal of Physical Oceanography **46**(3): 769-788.
- 405 Ye, R., C. Zhou, W. Zhao, J. Tian, Q. Yang, X. Huang, Z. Zhang and X. Zhao (2019). "Variability in the Deep



- 406 Overflow through the Heng-Chun Ridge of the Luzon Strait." Journal of Physical Oceanography **49**(3): 811-825.
- 407 Yuan, D. (2002). "A numerical study of the South China Sea deep circulation and its relation to the Luzon Strait
- 408 transport." Acta Oceanologica Sinica(2): 187-202.
- 409 Yuan, D. (2002). "A numerical study of the South China Sea deep circulation and its relation to the Luzon Strait
- 410 transport." Acta Oceanologica Sinica **21**(2): 187-202.
- 411 Zhang, Z., W. Zhao, J. Tian, Q. Yang and T. Qu (2015). "Spatial structure and temporal variability of the zonal flow
- 412 in the Luzon Strait." Journal of Geophysical Research: Oceans **120**(2): 759-776.
- 413 Zhu, Y. and X. Liang (2020). "Coupling of the Surface and Near-Bottom Currents in the Gulf of Mexico." J Geophys
- 414 Res Oceans **125**(11): e2020JC016488.
- 415 Zhu, Y., J. Sun, Y. Wang, Z. Wei, D. Yang and T. Qu (2017). "Effect of potential vorticity flux on the circulation in
- 416 the South China Sea." Journal of Geophysical Research: Oceans **122**(8): 6454-6469.
- 417
- 418